

# Vacuum Polarization Energy of the Kinks in the Sinh-Deformed Models.

I. Takyi, B. Barnes, J. Ackora-Prah

*Mathematics Department, Kwame Nkrumah University of Science and Technology, Kumasi, Ghana*

We compute the one-loop quantum corrections to the kink energies of the sinh-deformed  $\phi^4$  and  $\varphi^6$  models in one space and one time dimensions. These models are constructed from the well-known polynomial  $\phi^4$  and  $\varphi^6$  models by a deformation procedure. We also compute the vacuum polarization energy to the non-polynomial function  $U(\phi) = \frac{1}{4}(1 - \sinh^2 \phi)^2$ . This potential approaches the  $\phi^4$  model in the limit of small values of the scalar function. These energies are extracted from scattering data for fluctuations about the kink solutions. We show that for certain topological sectors with non-equivalent vacua the kink solutions of the sinh-deformed models are destabilized.

PACS numbers: 03.65.Ge, 05.45.Yv, 11.10.Lm, 21.10.Dr

## I. INTRODUCTION

Kinks are classical solutions to the non-linear field equations in one space and one time dimensions [1]. These kinks are referred to as topological kinks because they are characterized by a topological index which is related to their behavior at spatial infinity. In the quantized theory, this topological index becomes a conserved quantum number. In Skyrmon (a model for the baryon) [2–4] this conserved number is the baryon number. In one space and one time dimensions, this topological index arises as a result of distinct vacua kink solutions that interpolate neighboring vacua at negative and positive spatial infinity. In this case, the topological index translates into different masses for the fluctuations about the degenerate vacua.

An important property of the kink model is that in the classical picture it resembles an extended particle. Thus, it possesses localized energy densities. The integral of this energy is inversely proportional to its coupling constant and is identified as the mass of the particle. This mass overestimates the actual mass of the particle on the grounds that, quantum corrections are ignored. This is not a problem when investigating the properties of a single particle. In computations of the binding energies of compound objects such as hypernuclear atoms [5], the quantum corrections may become important when comparing configurations with different particle numbers. The vacuum polarization energies (VPE) is the leading quantum correction to the kink energies. We compute the VPE of the kink of sinh-deformed potentials using the spectral methods [6].

The VPE has been investigated by several researchers, for example the kinks in the  $\phi^4$  [7], and sine-Gordon models [8, 9], the Skyrmon as a model for baryons [10–12] and cosmic strings in the standard model [6, 13]. Recent studies in the  $\varphi^6$  model [14, 15] revealed that the VPE destabilized the kink as the kink produces different curvatures for the quantum fluctuations at both positive and negative spatial infinity. These instabilities of the kink have also been observed in the  $\phi^8$  model [16].

The non-polynomial models are another aspect where kink has played a major role. In Refs. [17, 18], the authors observed a pattern of kink-antikink scattering of the sinh-deformed models which was in consistent with the observation in polynomial models of the same order [19–23]. The study of this pattern amounts to numerically solving the equations of motion for time and space dependent fields with a specific initial conditions: in the distant past the kink and antikink are well separated and do not interact. When boosted with a prescribe velocity, the kink and antikink approach each other and interact at a later stage. This velocity is referred to as relative velocity between the kink and antikink. The patterns are observe for certain values of the relative velocity below a specific critical velocity. The remarkable physical phenomenon observed in their scattering analysis makes it interesting to further investigate other physical properties of it.

In this paper, we consider the non-polynomial hyperbolic potential of the  $\phi^4$  and  $\varphi^6$  types. We compute the VPE of the kink potentials in one space and one time dimensions for these models. These models have kink solutions similar to the polynomial  $\phi^4$  and  $\varphi^6$  models with spontaneous symmetry breaking. For this reason, we will compare the VPE results to the polynomial  $\phi^4$  and  $\varphi^6$  models to highlight their differences. The authors in Ref. [18] numerically studied the kink structures of the potential  $U(\phi) = \frac{1}{4}(1 - \sinh^2 \phi)^2$ . This potential mimic the  $\phi^4$  potential in the limit as the scalar function becomes small. We numerically compute the quantum corrections for this model and compare them to its polynomial counterpart.

We organized our work as follows: In the next section, we briefly review the general properties of static kinks with finite energy in one space and one time dimensions. We will review the method of computing the VPE in Section III. In Section IV we introduce the models we consider and present the numerical results in Section V. We conclude in Section VI.

## II. KINK CONCEPT

We consider a single scalar field  $\phi(x, t)$  in one space ( $x$ ) and one time ( $t$ ) dimensions, whose dynamics is defined by the Lagrangian density

$$\mathcal{L} = \frac{1}{2} (\phi_t)^2 - \frac{1}{2} (\phi_x)^2 - U(\phi), \quad (1)$$

where the subscripts,  $x$ ,  $t$ , denote differentiation with respect to  $x$  and  $t$ , respectively. Here,  $U(\phi)$  is the quantum field potential with two or more degenerate minima. The corresponding field equation for the Lagrangian is

$$\phi_{tt} - \phi_{xx} = -\frac{dU}{d\phi}. \quad (2)$$

For static configuration,  $\phi_t = 0$  and Eq.(2) reduces to

$$\phi_{xx} = \frac{dU}{d\phi}. \quad (3)$$

For finite energy, Eq.(3) transforms into a first-order differential equation

$$\frac{d\phi}{dx} = \pm \sqrt{2U(\phi)}. \quad (4)$$

In this case, the kink mass (classical energy) is given by

$$E[\phi] = \int \sqrt{2U(\phi)} d\phi, \quad (5)$$

where the integration boundaries are two neighboring potential minima.

To analyse the linear stability of the kink, we call the kink solution to the field equation  $\phi_K$  and parametrize the field

$$\phi(x, t) = \phi_K(x) + \eta(x, t).$$

By considering linear terms in  $\eta$  we get a Schrödinger-like equation in one dimension

$$[-\partial_x^2 + u(x)] \eta(x) = \omega^2 \eta(x), \quad (6)$$

where  $\eta(x)$  and  $\omega$  are eigenfunctions and eigenvalues of the Schrödinger operator  $H := -\partial_x^2 + u(x)$  and

$$u(x) = \left. \frac{d^2 U}{d\phi^2} \right|_{\phi_K(x)} \quad (7)$$

is the scattering potential which is generated by the background kink. At positive and negative spatial infinity for non-equivalent vacua,  $u(x)$  approaches a constant (so-called meson masses), i.e  $\lim_{x \rightarrow +\infty} u(x) = m_R^2$  and  $\lim_{x \rightarrow -\infty} u(x) = m_L^2$ . For non-equivalent vacua we take  $m_L \leq m_R$ . The analyses of the scattering potential sheds light on the scattering structure of the kink.

The sinh-deformed models are obtained from the known potentials  $U(\phi)$  to another potential  $V(\phi)$  by a deforming function  $g(\phi) = \sinh \phi$  [24–28],

$$V(\phi) = \frac{U(g(\phi))}{(g'(\phi))^2}. \quad (8)$$

The static solutions for the new potential  $V(\phi)$  is given by

$$\phi_K^{(\text{new})}(x) = g^{-1} \left( \phi_K^{(\text{old})}(x) \right), \quad (9)$$

where  $\phi_K^{(\text{old})}(x)$  is the static solution for the known potential  $U(\phi)$ .

### III. VACUUM POLARIZATION ENERGY

The VPE,  $E_{\text{vac}}$  is the leading quantum correction to the classical kink energy. It is the renormalized sum of the shifts of the zero-point energies of the quantum fluctuations due to their interaction with the background configuration generated by the kink. Formally the VPE reads

$$E_{\text{vac}} = \frac{1}{2} \sum_j^{\text{b.s.}} \omega_j + \frac{1}{2} \int_0^\infty dk \omega_k \Delta\rho(k) + E_{\text{ct}} \quad (10)$$

where the first term on the right hand side of Eq. (10) is contribution from the discrete bound states (b.s)  $\omega = \omega_j$  with  $|\omega_j| \leq m_L$  and the second term, is the continuum contribution weighted by the change in the density of states,  $\Delta\rho(k)$ . The third term on the right hand side of Eq. (10),  $E_{\text{ct}}$  is contribution from the counterterms that yields a finite results at one-loop level. Here  $\omega_k = \sqrt{k^2 + m_L^2}$  are the energies of the scattering states where  $k$  is the momentum and  $m_L$  is the mass of the mesons.

The modified density states  $\Delta\rho(k)$ , is measured by the derivative of the scattering eigen-phase shifts, extracted from the scattering matrix  $S(k)$

$$\Delta\rho(k) = \frac{1}{\pi} \frac{d}{dk} \delta(k), \quad \delta(k) = -\frac{i}{2} \ln [\det S(k)]. \quad (11)$$

We compute  $S(k)$  by introducing a pseudo-potential

$$u_p(x) = u(x) - m_L^2 + (m_L^2 - m_R^2) \Theta(x - x_m) \quad (12)$$

which vanishes at positive and negative spatial infinity. Here,  $\Theta(x)$  is the step function and  $x_m$  is an arbitrary matching point. Then the wave-equation becomes

$$[-\partial_x^2 + u_p(x)] \eta(x) = \begin{cases} k^2 \eta(x), & \text{for } x \leq x_m \\ q^2 \eta(x), & \text{for } x \geq x_m \end{cases} \quad (13)$$

where,  $q = \sqrt{\omega^2 - m_R^2}$ . Above threshold  $q$  is real so we take  $k \geq \sqrt{m_R^2 - m_L^2}$  and formulate a variable phase approach [29] by parametrizing

$$\begin{aligned} x \leq x_m : \eta(x) &= A(x) e^{ikx}, & A''(x) &= -2ikA'(x) + u_p(x)A(x) \\ x \geq x_m : \eta(x) &= B(x) e^{iqx}, & B''(x) &= -2iqB'(x) + u_p(x)B(x) \end{aligned} \quad (14)$$

where a prime denotes a derivative with respect to  $x$ . The boundary condition  $B(\infty) = A(-\infty) = 1$  and  $B'(\infty) = A'(-\infty) = 0$  solve Eq.(14) yielding the scattering matrix

$$S(k) = \begin{pmatrix} e^{-iqx_m} & 0 \\ 0 & e^{ikx_m} \end{pmatrix} \begin{pmatrix} B & -A^* \\ iqB + B' & ikA^* - A'^* \end{pmatrix}^{-1} \begin{pmatrix} A & -B^* \\ ikA + A' & iqB^* - B'^* \end{pmatrix} \begin{pmatrix} e^{ikx_m} & 0 \\ 0 & e^{-iqx_m} \end{pmatrix}, \quad (15)$$

where  $A = A(x_m)$ , etc. are the coefficient functions at the matching point. Below the threshold, i.e  $k \leq \sqrt{m_R^2 - m_L^2}$ ,  $q = i\kappa$  become imaginary with  $\kappa = \sqrt{m_R^2 - m_L^2 - k^2} \geq 0$ . We parametrize the wave equation for  $x \geq x_m$  as  $\eta(x) = B(x) e^{-i\kappa x}$ . This yields an ordinary differential equation

$$B''(x) = \kappa B'(x) + u_p(x)B(x).$$

We then extract the reflection coefficient via

$$S(k) = -\frac{A(B'/B - \kappa - ik) - A'}{A^*(B'/B - \kappa + ik) - A'^*} e^{2ikx_m}. \quad (16)$$

Adopting the no-tadpole renormalization scheme [15], the counterterm contribution in Eq.(10) subtracts exactly the Born approximation  $\delta^{(1)}$  from the phase shift [6]. For non-equivalent vacua with different mesons masses, there is a direct contribution from the pseudo-potential as well as from the step function potential

$$\delta^{(1)}(k) = -\frac{1}{2k} \int_{-\infty}^{\infty} dx u_p(x) \Big|_{x_m} + \frac{x_m}{2k} (m_R^2 - m_L^2) = -\frac{1}{2k} \int_{-\infty}^{\infty} dx u_p(x) \Big|_0, \quad (17)$$

where the subscript defines the position of the step in the pseudopotential  $u_p(x)$ . In the end, the Born approximation does not depend on  $x_m$ , even though  $u_p(x)$  was initially defined in terms of  $x_m$ . We then obtain the total VPE as

$$E_{\text{vac}} = \frac{1}{2} \sum_j (\omega_j - m_L) - \frac{1}{2\pi} \int_0^\infty dk \frac{k}{\sqrt{k^2 + m_L^2}} \left( \delta(k) - \delta^{(1)}(k) \right). \quad (18)$$

For reflection symmetric background potentials  $u(x) = u(-x)$  (i.e  $m_L = m_R$ ), the VPE is equivalently calculated by making use of analytic properties of scattering data and yields [6]

$$E_{\text{vac}}^S = \int_{m_L}^\infty \frac{dt}{2\pi} \frac{t}{\sqrt{t^2 - m_L^2}} \left[ \ln \left\{ g(0, t) \left( g(0, t) - \frac{1}{t} g'(0, t) \right) \right\} \right]_1. \quad (19)$$

The subscript indicates that the Born approximation has been subtracted. The function  $g(x, t)$  is the Jost solution factor on the imaginary axis that solves the differential equation

$$g''(x, t) = 2tg'(x, t) + V(x)g(x, t) \quad (20)$$

with boundary conditions  $g(\infty, t) = 1$  and  $g'(\infty, t) = 0$ .

#### IV. MODELS

Here we consider the models for our calculations. We make use of the natural units  $\hbar = c = 1$ .

##### A. The Sinh-Deformed Models

We consider the  $\phi^4$  and  $\varphi^6$  potentials

$$U_4 = \frac{1}{2} (\phi^2 - 1)^2 \quad \text{and} \quad U_6 = \frac{1}{2} (\varphi^2 + a^2) (\varphi^2 - 1)^2, \quad (21)$$

where we have scaled all coordinates, fields and coupling constants such that only the  $\varphi^6$  potential contains a single dimensionless parameter  $a$ . Applying the deformation procedure of Eq.(8) by using the deforming function  $g(\phi) = \sinh \phi$  ( $g(\varphi) = \sinh \varphi$  for the  $\varphi^6$  model) we obtain the potentials of the sinh-deformed  $\phi^4$  and  $\varphi^6$  models, respectively as

$$V_4 = \frac{1}{2} \text{sech}^2 \phi (1 - \sinh^2 \phi)^2 \quad \text{and} \quad V_6 = \frac{1}{2} \text{sech}^2 \varphi (\sinh^2 \varphi + a^2) (1 - \sinh^2 \varphi)^2. \quad (22)$$

There are two vacuum solutions in the sinh-deformed  $\phi^4$  model,  $\phi_0 = \pm \text{arsinh}(1)$  but for the sinh-deformed  $\varphi^6$  model, three cases emerges as observed from Figure 2. For  $a = 0$ , we observe three degenerate minima at  $\varphi_0 = 0$  and  $\varphi_0 = \pm \text{arsinh}(1)$ .

For  $0 < a^2 \leq \frac{1}{2}$ , an additional local minimum emerges at  $\varphi_0 = 0$  and finally, for  $a^2 > \frac{1}{2}$  we observe two degenerate minima at  $\varphi_0 = \pm \text{arsinh}(1)$ . The models in Eq. (22) possesses a discrete symmetry  $V_4(\phi) = V_4(-\phi)$  ( $V_6(\varphi) = V_6(-\varphi)$ ) that is broken by the perturbative vacua  $\phi_0 = \pm \text{arsinh}(1)$  (respectively,  $\varphi_0 = 0, \pm \text{arsinh}(1)$  in all three cases of the  $\varphi^6$  sinh-deformed model).

Applying Eq.(9) to the kink-antikink solutions of the polynomial  $\phi^4$  model [19] the kink-antikink solutions of the sinh-deformed  $\phi^4$  model are

$$\phi_{K, \bar{K}}(x) = \pm \text{arsinh}(\tanh(x)), \quad (23)$$

which are related by the spatial reflection  $x \leftrightarrow -x$ . The corresponding classical kink mass is

$$E_{\text{cl}} = \pi - 2. \quad (24)$$

The background potential for the fluctuations, which defines the excitation spectrum of the kink, is symmetric under the spatial reflection  $x \rightarrow -x$

$$v_4(x) = 2 \tanh^2 x + 1 + \frac{8 \tanh^2 x - 4}{(1 + \tanh^2 x)^2}. \quad (25)$$

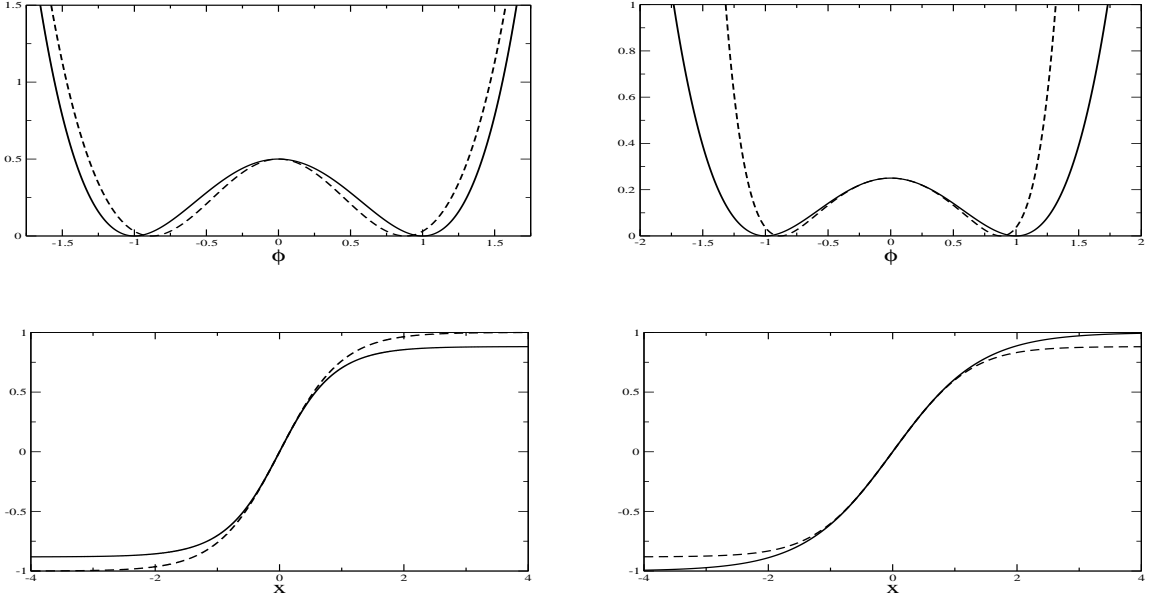


FIG. 1: Top row: field potentials of (left panel) the sinh-deformed (dashed line) (resp. polynomial (solid line)) and (right panel) hyperbolic (dashed line) (resp. polynomial (solid line)) of the  $\phi^4$  model. Bottom row: kink solutions of (left panel) the sinh-deformed (dashed line) (resp. polynomial (solid line)) and (right panel) hyperbolic (dashed line) (resp. polynomial (solid line)) of the  $\phi^4$  model.

This yield  $m_R = m_L$  with  $m_R = 2$ .

In the sinh-deformed  $\varphi^6$  model, we obtain the kink solution for  $a \neq 0$  as [14, 30]

$$\varphi_K = \operatorname{arsinh} \left[ a \frac{X - 1}{\sqrt{4X + a^2(1 + X)^2}} \right], \quad \text{with} \quad X = e^{m_R x} \quad (26)$$

where  $m_R = 2\sqrt{1 + a^2}$ . The spatial reflection  $x \rightarrow -x$  gives the antikink. The background potential is

$$\begin{aligned} v_6(x) = & 2(a^2 + \sinh^2 \varphi_K)(3 \sinh^2 \varphi_K - 1) + (\sinh^2 \varphi_K - 1)(9 \sinh^2 \varphi_K - 1) \\ & - 3(\sinh^2 \varphi_K - 1)^2 \tanh^2 \varphi_K - 6(a^2 + \sinh^2 \varphi_K)(\sinh^2 \varphi_K - 1) \tanh^2 \varphi_K \\ & + (a^2 + \sinh^2 \varphi_K)(\sinh^2 \varphi_K - 1)^2 (2 \sinh^2 \varphi_K - 1) \operatorname{sech}^4 \varphi_K \end{aligned} \quad (27)$$

and is symmetric under the spatial reflection  $x \rightarrow -x$ . Consequently,  $v_6(-\infty) = v_6(\infty)$  and  $m_L = m_R$ .

For  $a = 0$ , two distinct kink solutions exist [19, 23]. The first one interpolates between  $\varphi_0 = 0$  and  $\varphi_0 = \operatorname{arsinh}(1)$ ,

$$\varphi_{K_I} = \operatorname{arsinh} \left( \sqrt{\frac{1}{2}(1 + \tanh x)} \right) \quad (28)$$

while the second one interpolates between  $\varphi_0 = -\operatorname{arsinh}(1)$  and  $\varphi_0 = 0$ ,

$$\varphi_{K_{II}} = -\operatorname{arsinh} \left( \sqrt{\frac{1}{2}(1 - \tanh x)} \right). \quad (29)$$

The corresponding classical kink mass in either case is

$$E_{\text{cl}} = \frac{1}{2} (2 \ln 2 - 1). \quad (30)$$

The background potential for the fluctuations in this case is not symmetric under the spatial reflection  $x \rightarrow -x$

$$v_6(x) = 2 \tanh^2 x + 5 \tanh x - 7 + \frac{10 \tanh^2 x + 54}{(3 + \tanh^2 x)^2}. \quad (31)$$

This, of course, implies that  $m_R = 2 \neq m_L = 1$ .

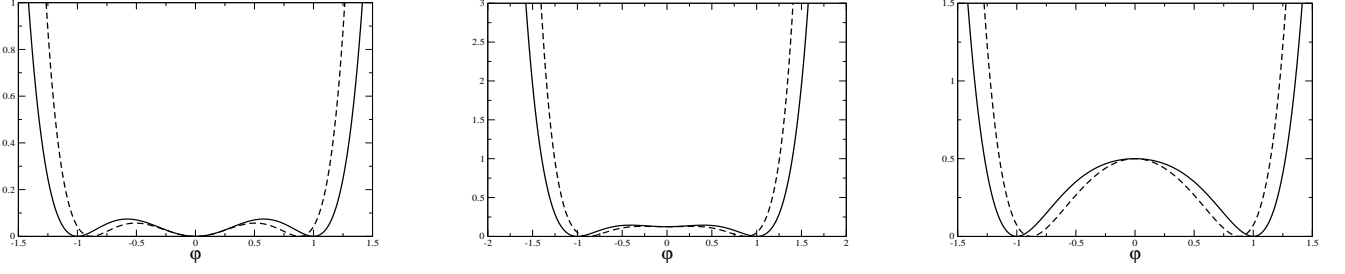


FIG. 2: The field potentials of the sinh-deformed  $\varphi^6$  model (dashed lines) and polynomial  $\varphi^6$  model (solid lines) for various values of the dimensionless parameter. From left to right  $a = 0, 0.5, 1$ .

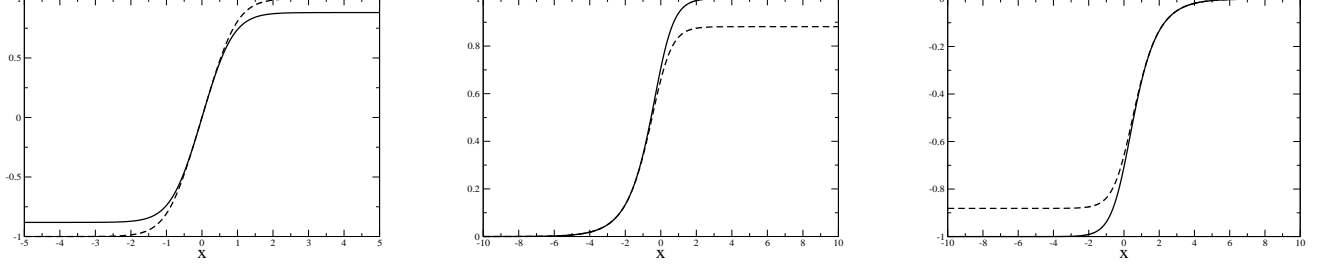


FIG. 3: The kink solutions of the sinh-deformed  $\varphi^6$  model (dashed lines) and polynomial  $\varphi^6$  model (solid lines). From left to right: eq(26) for  $a = 1$ , eq(28) and eq(29) for  $a = 0$ .

## B. The Hyperbolic Model

Here we consider the hyperbolic potential [31]

$$V(\phi) = \frac{1}{4} (1 - \sinh^2(\phi))^2. \quad (32)$$

This potential has two degenerate minima  $\phi_0 = \pm \text{arsinh}(1)$ . In the limit of small values of  $\phi$ , this potential approaches the polynomial  $\phi^4$  model

$$U(\phi) = \frac{1}{4} (1 - \phi^2)^2, \quad (33)$$

with a factor  $\frac{1}{2}$  compared to  $U_4$  in Eq. (21). The kink-antikink solutions of the hyperbolic  $\phi^4$  model are

$$\phi_{K,\bar{K}}(x) = \pm \text{artanh}\left(\frac{1}{\sqrt{2}} \tanh(x)\right), \quad (34)$$

which are related by the spatial reflection  $x \leftrightarrow -x$ . The resulting classical mass is

$$E_{\text{cl}} = \frac{3}{8} \sqrt{2} \left\{ \ln(2\sqrt{2} + 3) - \ln(-2\sqrt{2} + 3) \right\} - 1. \quad (35)$$

The background potential

$$v(x) = 2 + \frac{14 \tanh^2(x) - 12}{(\tanh^2(x) - 2)^2} \quad (36)$$

is symmetric under the spatial reflection  $x \leftrightarrow -x$ . In the limit as  $x \rightarrow \pm\infty$  we have  $m_L = m_R = 2$ .

## V. NUMERICAL RESULTS

In this section, we report our numerical results for the VPEs for the two models discussed above. As stated earlier, we have rescaled to dimensionless coordinates and fields such that model parameters (coupling constant ‘ $\lambda$ ’ and mass

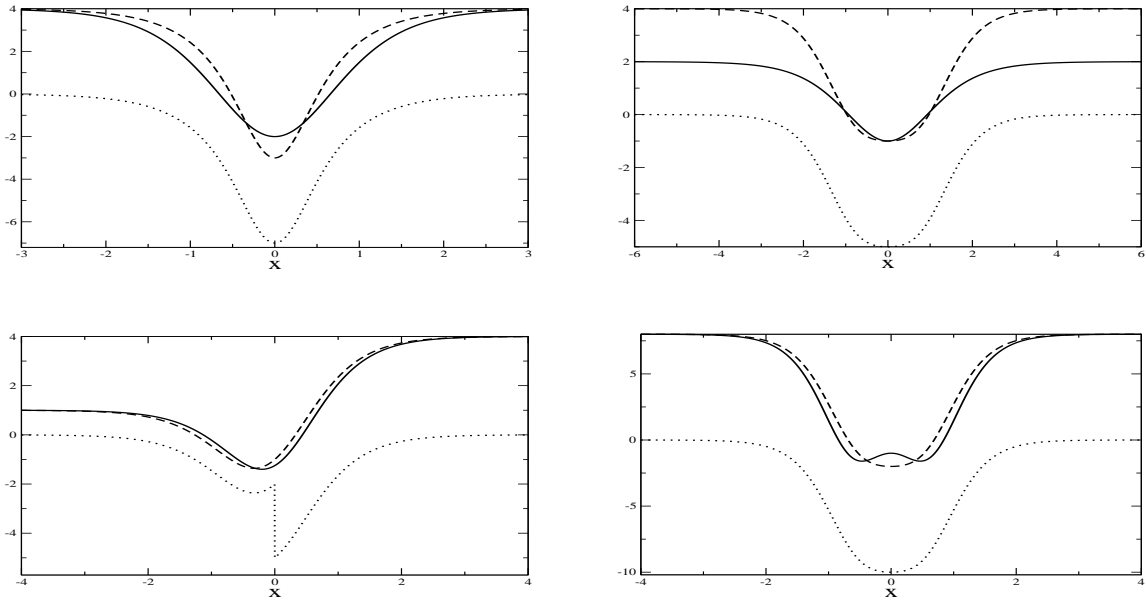


FIG. 4: The scattering (dashed lines) and pseudo (dotted lines) potentials for the various models. The scattering potential for the corresponding polynomial model for the various models is indicated with the solid lines. Top row: the sinh-deformed (left panel) and hyperbolic (right panel)  $\phi^4$  models. Bottom row: the sinh-deformed  $\phi^6$  model for  $a = 0$  (left panel) and for  $a = 1$  (right panel).

‘ $m$ ’) are unity. It must be noted that the coupling constant  $\lambda$  serves as a loop-counting parameter. In this case, the classical mass scales as  $\frac{1}{\lambda}$  while the VPE proportional to  $m$ , where  $m$  is a mass parameter<sup>1</sup> in the potentials considered. Thus, taking the coupling constant as unity does not affect the computation of the VPE.

We obtain the bound states energies contribution to the VPE, by first solving the Schrödinger-wave equation using the Boole’s algorithm, which is otherwise known as the 5-point closed Newton-Cote formula; with the initial conditions

$$\eta_R \rightarrow 1, \quad \eta'_R \rightarrow -\sqrt{m_R^2 - m_L^2 - E^2} \quad \text{as } x \rightarrow \infty$$

and

$$\eta_L \rightarrow 1, \quad \eta'_L \rightarrow \sqrt{m_L^2 - E^2} \quad \text{as } x \rightarrow -\infty.$$

from either side. We obtained the bound state energy by tuning the energy  $\omega = \omega_j$  such that the Wronskian  $\eta_L \eta'_R - \eta_R \eta'_L$  is zero at the matching point  $x_m$ .

The next step requires computing the continuum part of the VPE, where the phase shift and its first Born approximation are obtained by solving Eqs. (11) and (17). We achieved this by utilizing the Runge Kutta algorithm to solve Eq. (14) which yields the S-matrix needed for the computation of the phase shift. It must be noted that the numerically obtained phase shift does not vary with the choice of  $x_m$ .

We will be looking at two scenarios in the computation of the VPE. The first case deals with models with symmetric scattering potential. This regime, has equivalent vacua at  $x \rightarrow \pm\infty$ , as such translating the kink solution as<sup>2</sup>  $x \rightarrow x + x_0$  does not change the VPE of the kink. For models with asymmetric scattering potential, the non-equivalent vacua produce translational variance with the center of the kink solution  $x_0$ .

<sup>1</sup> This generally holds for the  $\phi^4$  model. For this to be correct, for the  $\phi^6$  model the dimensionless parameter  $a$  must be written as  $a = \alpha \sqrt{\frac{m}{\lambda}}$  where  $\alpha$  do not vary with  $m$  or  $\lambda$ . Then the quadratic mass type term in  $U_6(\phi)$  does not contain the coupling constant  $\lambda$ .

<sup>2</sup> This corresponds to kink solution centered at  $-x_0$ .

	bound state energies		$E_{b.s}$	$E_{scat.}$	$E_{vac.}$
polynomial $\phi^4$	0.0	1.732	-1.134	0.470	-0.664(-0.666)
sinh-deformed $\phi^4$	0.0	1.892	-1.054	0.412	-0.643(-0.644)

TABLE I: The bound state energies and VPEs of the sinh-deformed  $\phi^4$  model cf. Eq. (22) and polynomial  $\phi^4$  model cf. Eq. (21). The entries  $E_{b.s}$  and  $E_{scat.}$  denote the bound state and continuum contributions to the VPE, *i.e.* the two distinct terms in Eq. (18). The last entry in parenthesis are the Jost solutions cf. Eq. (19) confirming the VPE result.

TABLE II: The VPE as a function of the center of the kink  $x_0$  in the polynomial  $\varphi^6$  model and sinh-deformed  $\varphi^6$  model cf. Eq. (22) for  $a = 0$ .

	$E_{vac}$				
$x_0$	-2	-1	0	1	2
polynomial $\varphi^6$	0.154	0.053	-0.047	-0.148	-0.249
sinh-deformed $\varphi^6$	0.229	0.129	0.028	-0.074	-0.176

### A. The Sinh-Deformed Models

We first compare the results of the sinh-deformed  $\phi^4$  model and its corresponding polynomial model. The two vacua for both models have equal curvature with  $m_L = 2$ . From the top left panel of figure 4, one observes that the scattering potential of the polynomial  $\phi^4$  model is shallower and broader than that of the polynomial  $\phi^4$  model. We observed that both cases have two bound states with the bound state energies of the polynomial  $\phi^4$  model smaller than that of the corresponding sinh-deformed model; this is attributed to the shallowness and broadness of its scattering potential. This in effect accounts for the smaller value of the VPE observed in the polynomial  $\phi^4$  model as indicated in table I.

In the case of sinh-deformed  $\varphi^6$  model for  $a = 0$ , we have an asymmetric scattering potential with an unequal meson masses  $m_L = 1$  and  $m_R = 2$  for the kink soliton cf. Eq. (28). We observed from the bottom left of figure 4 for  $a = 0$  that the scattering potential is narrower and almost overlap that of its polynomial counterpart. This in turn causes its VPE to be large cf. table II. Furthermore, the results indicate that except for the zero-mode there will be no additional bound state. We numerically obtained the binding energy (denoted by  $E_{b.s}$ ), as  $E_{b.s} = -0.4107$  which is larger than the binding energy,  $E_{b.s} = -0.5$  of the polynomial  $\varphi^6$  model. The unequal meson masses produces a translational variance of the VPE as seen in table II under the translation  $x \rightarrow x + x_0$ . The results show that as  $x_0$  increases, the kink shifts the vacuum with the bigger mass towards negative infinity causing low-lying modes to disappear. This decreases the VPE. It must be noted that the results stem from a change in values of the phase shift as  $x_0$  varies. The phase shift exhibits the threshold scattering cusp  $k = \sqrt{m_R^2 - m_L^2} = \sqrt{3}$  and approaches  $\frac{\pi}{2}$  as  $k \rightarrow 0$  confirming Levinson's theorem.

For  $a \neq 0$  we observe a symmetric scattering potential cf. the bottom right in figure 4. This potential is narrower compared to that of the polynomial  $\varphi^6$  model. In effect yields large values for the VPEs for various values of  $a$  as seen in table III. Furthermore, we have also confirmed the VPE results using the Jost function formalism of Eq. (19).

### B. The Hyperbolic Model

We observe that the scattering potential of the hyperbolic  $\phi^4$  model is symmetric and broader than its corresponding polynomial model. This causes its VPE to be smaller compared to the polynomial counterpart as seen in table IV. Also, we observe two vibrational modes in addition to the translational zero-mode compared to the one vibrational mode of its polynomial model. The occurrence of this is due to the broadness of its scattering potential. Finally, the VPE result from calculations of the hyperbolic model is in agreement (within numerical precision) to the one

TABLE III: The VPEs for the symmetric scattering potential of the polynomial and sinh-deformed  $\varphi^6$  models for  $a \neq 0$ .

$a$	0.01	0.05	0.1	0.2	1.0	1.5
polynomial $\varphi^6$	-1.841	-1.596	-1.462	-1.297	-1.102	-1.297
sinh-deformed $\varphi^6$	-1.819	-1.570	-1.430	-1.256	-1.037	-1.230
Jost solutions	-1.827	-1.576	-1.435	-1.261	-1.038	-1.229



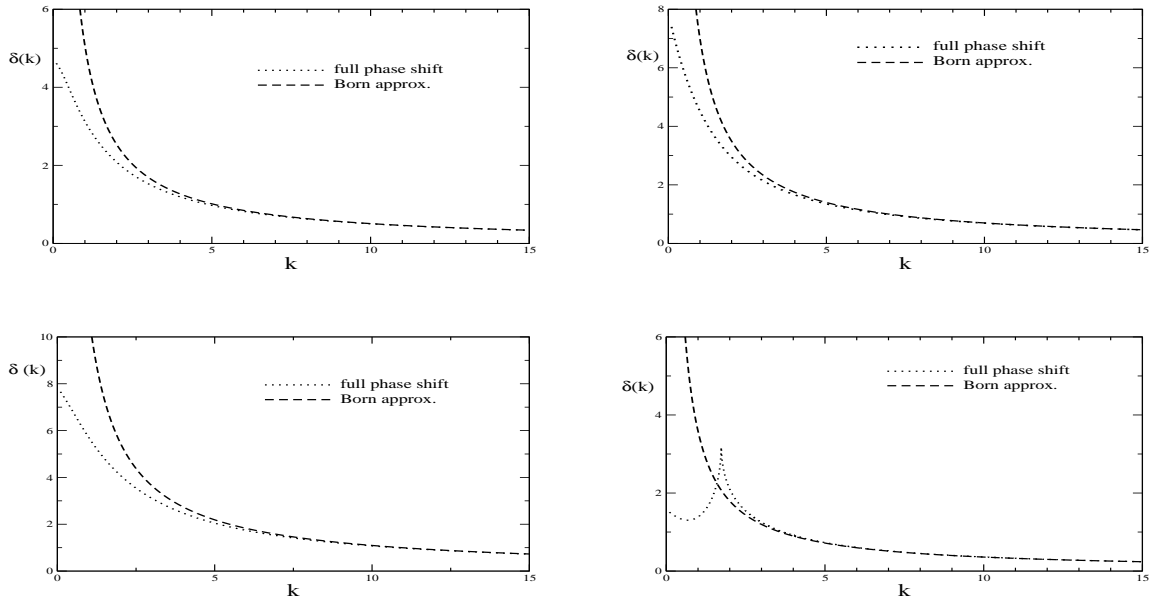


FIG. 5: Phase shifts for the various models. Top row: sinh-deformed (left panel) and hyperbolic (right panel)  $\phi^4$  models. Bottom row sinh-deformed  $\phi^6$  models for:  $a \neq 0$  (left panel) and  $a = 0$  (right panel).

	bound state energies			$E_{b,s}$	$E_{scat.}$	$E_{vac.}$
polynomial $\phi^4$	0.0	1.225		-0.802	0.354	-0.448(-0.471)
hyperbolic $\phi^4$	0.0	1.433	1.911	-1.328	0.597	-0.732(-0.734)

TABLE IV: The bound state energies and VPEs of the hyperbolic  $\phi^4$  model cf. Eq. (32) and polynomial  $\phi^4$  model cf. Eq (33). We have confirmed the VPE result using the Jost function formalism of Eq. (19) which is indicated in the parenthesis of the last entry.

obtained by using the heat kernel method [32, 33]. The result from the heat kernel method has the value of VPE as  $E_{vac} = -0.73433$ .

## VI. CONCLUSION

We have investigated the vacuum polarization energies (VPE) of kinks in the sinh-deformed  $\phi^4$  and  $\phi^6$  models obtained from the polynomial  $\phi^4$  and  $\phi^6$  models by a deformation procedure. We make use of spectral methods for computing the VPE in terms of scattering data for the quantum fluctuations about the classical kink. The models we used are not multiplicatively renormalizable. However, using the no-tadpole renormalization condition at one-loop order produce finite results for our calculations.

Our results show that the sinh-deformed  $\phi^4$  and  $\phi^6$  models show similar behaviors to their polynomial counterparts. In the case of the  $\phi^4$  model they both have two bound states; the zero-mode and a vibrational shape mode. The narrowness of the scattering potential of the sinh-deformed  $\phi^4$  model causes its vibrational mode frequency to be larger than that of its polynomial counterpart. In effect, the VPE of the sinh-deformed model is quite large. In the case of the  $\phi^6$  model with the dimensionless parameter  $a = 0$ , the kink solutions of both models possesses non-equivalent vacua at spatial infinity. This leads to translational variance with respect to the center of the kink. The VPE may assume any negative value which then destabilizes the kink. The broadness of the scattering potential of the polynomial model in this case, causes its binding energy to be smaller than that of the sinh-deformed model.

In the case of the hyperbolic  $\phi^4$  model, we find its scattering potential to be broader than its polynomial counterpart. We also observe two vibrational modes for the hyperbolic model as compared to only one for its polynomial counterpart. In effect, the VPE of the hyperbolic  $\phi^4$  model is smaller. The reported value of the VPE in this case, is  $E_{vac} = -0.734$  which is in agreement with the value reported using the heat kernel method. The later approach makes use of  $\zeta$ -function regularization which requires truncation approximation.

It will be interesting to study the VPEs as a function of the kink-antikink potentials of the sinh-deformed models as well as the hyperbolic  $\phi^4$  model. To do this requires to first substitute the configuration of the kink-antikink solutions

that describe its scattering interactions to the Lagrangian density to obtain the classical kink potential. The VPE is then computed using the obtained potential. In deriving this configuration care must be taken in such a way that the configuration is not a solution to the stationary equations and additions must be made to avoid an imaginary VPE.

### Acknowledgements

We are grateful to H. Weigel for stimulating discussions and helpful comments on the manuscripts.

- 
- [1] R. Rajaraman, *Solitons and Instantons*, (North Holland, 1982).
  - [2] T. H. R. Skyrme *Int. J. Mod. Phys. A* **3**, 2745 (1988) 2745. Article reconstructed by I. Aitchison.
  - [3] G. S. Adkins, C. R. Nappi, and E. Witten, *Nucl. Phys. B* **228**, 552 (1983).
  - [4] H. Weigel, *Lect. Notes Phys.* **743**, 1 (2008).
  - [5] E. F. Meoto, M. L. Lekala, G. J. Rampho and B. Mukeru, *J. Phys. G* **46**, 095102 (2019).
  - [6] N. Graham, M. Quandt and H. Weigel *Lect. Notes Phys.* **777**, 1 (2009).
  - [7] R. F. Dashen, B. Hasslacher and A. Neveu, *Phys. Rev. D* **10**, 4130 (1974).
  - [8] R. F. Dashen, B. Hasslacher and A. Neveu, *Phys. Rev. D* **11**, 3424 (1975).
  - [9] L. D. Faddeev and V. E. Korepin, *Phys. Rep.* **42**, 1 (1978).
  - [10] B. Moussallam and D. Kalafatis, *Phys. Lett. B* **272**, 196 (1991).
  - [11] G. Holzwarth and H. Walliser, *Nucl. Phys. A* **587**, 721 (1995).
  - [12] F. Meier and H. Walliser, *Phys. Rep.* **289**, 383 (1997).
  - [13] A. Achúcarro and T. Vachaspati, *Phys. Rep.* **327**, 347 (2000).
  - [14] H. Weigel, *Adv. High Energy Phys.* **2017**, 1486912 (2017).
  - [15] H. Weigel, *Phys. Lett. B* **766**, 65 (2017).
  - [16] I. Takyi, M. K. Matfunjwa and H. Weigel, *Phys. Rev. D* **102**, 116004 (2020).
  - [17] D. Bazeia, E. Belendryasova and V. A. Gani, *Eur. Phys. J. C* **78**, 340 (2018).
  - [18] D. Bazeia, A. R. Gomes, K. Z. Nobrega, F. C. Simas, *Int. J. Mod. Phys. A* **34**, 1950200 (2019).
  - [19] I. Takyi and H. Weigel, *Phys. Rev. D* **94**, 8 (2016).
  - [20] H. Weigel, *J. Phys. Conf. Ser.* **482**, 012045 (2014).
  - [21] P. Anninos, S. Oliveira, R. H. Matzner, *Phys. Rev. D* **44**, 1147 (1991).
  - [22] D. K. Campbell, J. F. Schonfeld and C. A. Wingate, *Physica D* **9**, 1 (1983).
  - [23] P. Dorey, K. Mersh, T. Romanczukiewicz, Y. Shnir, *Phys. Rev. Lett.* **107**, 091602 (2011).
  - [24] D. Bazeia, M. A. González León, L. Losano and J. M. Guilarte, *Phys. Rev. D* **73**, 105008 (2006).
  - [25] D. Bazeia, L. Losano and J. M. C. Malbouisson, *Phys. Rev. D* **66**, 101701 (2002).
  - [26] C. A. Almeida, D. Bazeia, L. Losano and J. M. C. Malbouisson, *Phys. Rev. D* **69**, 067702 (2004).
  - [27] D. Bazeia and L. Losano, *Phys. Rev. D* **73**, 025016 (2006).
  - [28] D. Bazeia, E. E. M. Lima and L. Losano, *Int. J. Mod. Phys. A* **32**, 1750163 (2017).
  - [29] F. Calegero, *Variable Phase Approach to Potential Scattering*, (Acad. Press, New York and London, 1967).
  - [30] M. A. Lohe, *Phys. Rev. D* **20**, 3120 (1979).
  - [31] D. Bazeia, D. A. Ferreira, E. E. M. Lima and L. Losano, *Annals Phys.* **395**, 275 (2018).
  - [32] A. Alonso-Izquierdo and J. Mateos Guilarte, *Nucl. Phys. B* **852**, 696 (2011).
  - [33] A. Alonso-Izquierdo and J. Mateos Guilarte, *Annals Phys.* **327**, 2251 (2012).